International Journal of Minerals, Metallurgy and Materials
Accepted manuscript, https://doi.org/10.1007/s12613-024-3021-6

Temperature-stabilized novel high-entropy microwave dielectric $(Mg_{1/2}Zn_{1/2})_{0.4+x}Li_{0.4}(Ca_{1/2}Sr_{1/2})_{0.4-x}TiO_3$ ceramics

Xingyue Liao[1)], *Yuanming Lai*[1),✉], *Huan Huang*[1)], *Mingjun Xie*[1)], *Weiping Gong*[2)], *Yuanxun Li*[3)], *Qian Liu*[1)], *Chongsheng Wu*[1)], *Jiao Han*[4)], *and Yiming Zeng*[4)]

1) School of Mechanical and Electrical Engineering, Chengdu University of Technology, Chengdu 610059, China

2) Guangdong Provincial Key Laboratory of Electronic Functional Materials and Devices, Huizhou University, Huizhou 516001, China

3) State Key Laboratory of Electronic Thin Films and Integrated Devices, University of Electronic Science and Technology of China, Chengdu 610054, China

4) Yunnan Precious Metals Lab Co.,LTD, Kunming 650106, China

Corresponding author: Yuanming Lai E-mail: laiyuanming19@cdut.edu.cn

Abstract: In this work, a series of high-entropy ceramics which nominal composition $(Mg_{1/2}Zn_{1/2})_{0.4+x}Li_{0.4}(Ca_{1/2}Sr_{1/2})_{0.4-x}TiO_3$ ($0 \leq x \leq 0.4$) have been successfully synthesized using the conventional solid-phase method. The $(Mg_{1/2}Zn_{1/2})_{0.4+x}Li_{0.4}(Ca_{1/2}Sr_{1/2})_{0.4-x}TiO_3$ ceramics were confirmed to be composed of the main phase (Zn, Mg, Li)TiO_3 and the secondary phase $Ca_{0.5}Sr_{0.5}TiO_3$ by XRD, Rietveld refinement and EDS analysis. The quality factor (*Qf*) of the samples is inversely proportional to the content of the $Ca_{0.5}Sr_{0.5}TiO_3$ phase, and it is influenced by the density. The secondary phase and molecular polarizability (α_T) have a significant impact on the dielectric constant (ε_r) of the samples. Moreover, the temperature coefficient of resonant frequency (τ_f) of the samples is determined by the distortion of [TiO_6] octahedra and the secondary phase with a positive τ_f value. $(Mg_{1/2}Zn_{1/2})_{0.4+x}Li_{0.4}(Ca_{1/2}Sr_{1/2})_{0.4-x}TiO_3$ ceramics achieved ideal microwave dielectric properties (ε_r = 17.6, *Qf* = 40,900 GHz, τ_f = -8.6 ppm/°C) when x = 0.35. Therefore, $(Mg_{1/2}Zn_{1/2})_{0.4+x}Li_{0.4}(Ca_{1/2}Sr_{1/2})_{0.4-x}TiO_3$ ceramics possess the potential for application in wireless communication, and a new approach has been provided to enhance the performance of microwave dielectric ceramics.

Keywords: high-entropy ceramics; $MgTiO_3$-based ceramics; microwave dielectric properties; Near-zero τ_f value

1. Introduction

Microwave dielectric ceramics are widely utilized in microwave resonators, filters, oscillators, phase shifters, and substrates [1]. Currently, the miniaturization, chip integration, and consolidation of microwave devices are key trends in development. The advancement of cutting-edge wireless communication technology, represented by 5G, has put forward higher and newer requirements for the performance of microwave dielectric ceramics. One of the keys focus in recent years has been the development of microwave dielectric ceramics with low loss, relatively high dielectric constants (ε_r, 20-100), and near-zero temperature coefficient of resonant frequency (τ_f) [2,3].

"High-entropy" as a novel material design method, has greatly enriched the material system and also provided an avenue for high-performance dielectric materials required in wireless communication systems [4]. Lu et al. [5] proposed to combine BCC and FCC phases to form multiphase high-entropy alloys to obtain a significant increase in the overall performance of the materials. Currently according to phase composition can be categorized into several types of single-phase, two-phase, and multi-phase high entropy alloys. The concept of "entropy engineering" involves designing materials by controlling configurational entropy [6]. According to the Gibbs free energy (G) equation: $G = H - TS$, where H is enthalpy, T is temperature, and S is configurational entropy. In general, a system with the S greater than or equal to 1.5R is a high-entropy material [7]. A novel high entropy ceramic $(Mg_{0.2}Ni_{0.2}Zn_{0.2}Co_{0.2}Mn_{0.2})_2SiO_4$ using traditional solid-state methods, achieving excellent microwave dielectric properties (ε_r = 8.02, tanδ = 0.00051 at 14.5 GHz, and τ_f = −38.2 ppm/°C) [8]. The perovskite-type high entropy $(La_{0.2}Li_{0.2}Ba_{0.2}Sr_{0.2}Ca_{0.2})TiO_3$ ceramics obtained a high dielectric constants (ε_r = 230) [9]. Based on high-entropy strategies, the $Li(Gd_{0.2}Ho_{0.2}Er_{0.2}Yb_{0.2}Lu_{0.2})GeO_4$ ceramic

was synthesized and achieved a near-zero τ_f value (-2.9 ppm/°C) [10]. These results indicate that the high-entropy compositional could provide innovative approaches for improving the temperature stability and other properties of microwave dielectric ceramics.

Compared to MTiO$_3$ (M = Mn, Ni, and Co), the ilmenite-structured MgTiO$_3$ demonstrates exceptional microwave dielectric properties among low-loss ceramic materials [11]. However, the large negative τ_f value of MgTiO$_3$ (MT) (τ_f = -50 ppm/°C) ceramics, and the high sintering temperature (about 1450 °C) limits its practical application [12–14]. Blending compounds with opposite τ_f value is one of efficient ways to achieve a τ_f value close to zero. Such as the $(1-x)$Mg$_2$TiO$_4$-xSrTiO$_3$ ceramics with a near-zero τ_f value of -3.3 ppm/°C, but it still exhibited a high sintering temperature of 1440 °C [15].

The positive τ_f value in CaTiO$_3$ and SrTiO$_3$ can be used to adjust the τ_f value of MgTiO$_3$ ceramics [16]. Furthermore, the incorporation of Li element into (Mg$_{0.2}$Co$_{0.2}$Ni$_{0.2}$Cu$_{0.2}$Zn$_{0.2}$)O ceramics increase the relative ε_r value and Zn element can improve the quality factor (Qf) of MgTiO$_3$ ceramics [17,18]. This study aims to achieve a near-zero τ_f value and reduce the densification temperature while maintaining a high Qf value and dielectric constant. Based on the above performance, ionic radius, and valence considerations, a nominal composition of $(Mg_{1/2}Zn_{1/2})_{0.4+x}Li_{0.4}(Ca_{1/2}Sr_{1/2})_{0.4-x}TiO_3$ (x = 0, 0.1, 0.2, 0.3, 0.325, 0.35, 0.375, 0.4) was designed for the five-component high-entropy ceramics. The sintering behavior, phase composition, microstructure, and microwave dielectric properties of $(Mg_{1/2}Zn_{1/2})_{0.4+x}Li_{0.4}(Ca_{1/2}Sr_{1/2})_{0.4-x}TiO_3$ ceramics were investigated.

2. Experimental Procedure

The $(Mg_{1/2}Zn_{1/2})_{0.4+x}Li_{0.4}(Ca_{1/2}Sr_{1/2})_{0.4-x}TiO_3$ ($0 \le x \le 0.4$) ceramics were prepared using the solid-phase reaction method. The analytically pure raw materials including MgO, ZnO, Li_2CO_3, $SrCO_3$, $CaCO_3$, and TiO_2 were weighed according to the stoichiometric ratio of $(Mg_{1/2}Zn_{1/2})_{0.4+x}Li_{0.4}(Ca_{1/2}Sr_{1/2})_{0.4-x}TiO_3$ (x = 0, 0.1, 0.2, 0.3,

0.325, 0.35, 0.375, 0.4). The weighed powders were then placed in a ball milling jar containing a certain proportion of zirconia balls, added with a suitable amount of deionized water, and ball-milled at a speed of 250 r/min for 4 h. Then dry the slurry at 100 °C and pre-sinter it at 1150 °C for 4 h. After pre-sintering, the powders were subjected to secondary ball milling and dried at 100 ℃ for 12 h. PVA (10 wt%) solution was added to the dried powders with thorough mixing. Subsequently, under a pressure of 20 MPa, press the mixture into a disk with a diameter of 12 millimeters and a thickness of 6 millimeters. The formed discs were placed in a high-temperature sintering furnace, heated at a rate of 5 °C/min to 600 °C, kept at this temperature for 4 h for debinding, and then sintered at 1200 °C~1350 °C for 4 h to obtain the final samples.

The obtained samples were tested for crystalline phase employing an X-ray diffractometer (XRD, Cu Kα, Discover 8, Germany) with a scanning range of 2θ = 10°~120°. Using the Rietveld refinement method, crystal structure parameters were obtained based on XRD data using the Fullprof program [19]. Scanning electron microscopy (SEM, SU8010N, Hitachi, Japan) was utilized to evaluate the surface morphology and thermal etching of the polished samples. Energy dispersive X-ray spectroscopy (EDS) was applied to detect the composition of the samples. The densification of the samples was evaluated by the following equation [20,21]:

$$\rho_{re} = \frac{\rho_{bulk}}{\rho_{th}} \tag{1}$$

Where ρ_{re} is the relative density of the samples, utilizing the Archimedes principle, the bulk density (ρ_{bulk}) is calculated, while the theoretical density (ρ_{th}) is computed according to the subsequent equation [20,21]:

$$\rho_{1,2\text{th}} = \frac{A \times Z}{N \times V} \tag{2}$$

where the volume of the unit cell (V), Avogadro's number (N), atomic weight (A), and the number of atoms in the unit cell (Z) are represented by V, N, A, and Z, respectively.

According to the following equation, the theoretical density (ρ_{th}) in a multi-phase ceramic system can be calculated [22]:

$$\rho_{\text{th}} = \left(w_1 + w_2\right)\left(\frac{w_1}{\rho_{1\text{th}}} + \frac{w_2}{\rho_{2\text{th}}}\right)^{-1} \tag{3}$$

in the equation, ω_1, ω_2, ρ_{1th}, and ρ_{2th} denote the weight fraction and theoretical density of each phase, respectively. Using a network analyzer (Agilent Technologies, Agilent E5072A, USA), the microwave dielectric properties of the samples were measured. The τ_f value can be obtained from the given equation [23]:

$$\tau_f = \frac{f_2 - f_1}{60 \times f_1} \times 10^6 \left(ppm/℃\right) \tag{4}$$

where f_1 and f_2 denote the resonant frequencies at 25 °C and 85 °C, respectively.

3. Results and discussion

3.1. Phase composition

The XRD patterns of the ceramics sintered at 1200 °C for 4 h, $(Mg_{1/2}Zn_{1/2})_{0.4+x}Li_{0.4}(Ca_{1/2}Sr_{1/2})_{0.4-x}TiO_3$ ($0 \le x \le 0.4$), are shown in Fig. 1. The XRD patterns of $(Mg_{1/2}Zn_{1/2})_{0.4+x}Li_{0.4}(Ca_{1/2}Sr_{1/2})_{0.4-x}TiO_3$ ($0 \le x \le 0.375$) ceramics can be indexed to $ZnTiO_3$ (PDF #39-0190) with a cubic structure as the main phase. Additionally, a secondary phase of $(Ca_{0.5}Sr_{0.5})TiO_3$ (PDF #89-8032) was also observed. When x = 0.4, the secondary phase of $(Mg_{1/2}Zn_{1/2})_{0.4+x}Li_{0.4}(Ca_{1/2}Sr_{1/2})_{0.4-x}TiO_3$ ceramics consists of small amounts of Mg_2TiO_4 and $MgTi_2O_5$. The main reaction processes of $(Mg_{1/2}Zn_{1/2})_{0.4+x}Li_{0.4}(Ca_{1/2}Sr_{1/2})_{0.4-x}TiO_3$ ($0 \le x \le 0.375$) ceramics can be described as the following equations:

$$2ZnO + 3TiO_2 \rightarrow Zn_2Ti_3O_8 \tag{5}$$

$$Zn_2Ti_3O_8 \rightarrow 2ZnTiO_3 + TiO_2 \tag{6}$$

$$CaCO_3 \rightarrow CaO + CO_2(g) \tag{7}$$

$$SrCO_3 \rightarrow SrO + CO_2(g) \tag{8}$$

$$CaO + SrO + 2TiO_2 \rightarrow 2Ca_{0.5}Sr_{0.5}TiO_3 \tag{9}$$

ZnO and TiO_2 chemically react at a lower temperature (800 ℃) to produce unstable $Zn_2Ti_3O_8$ [24,25], and as the sintering temperature rises $Zn_2Ti_3O_8$ decomposes into $ZnTiO_3$ and TiO_2. A small amount of $Zn_2Ti_3O_8$ may be generated during the temperature reduction process. So very little $Zn_2Ti_3O_8$ is present in the XRD patterns. In Fig. 1, it is evident that the intensity of the (020) diffraction peaks decreases as $(Ca_{1/2}Sr_{1/2})^{2+}$ decreases, with no significant shifts observed in any of the diffraction peaks.

To confirm the phase composition of $(Mg_{1/2}Zn_{1/2})_{0.4+x}Li_{0.4}(Ca_{1/2}Sr_{1/2})_{0.4-x}TiO_3$ ceramics, Fig. 2(a) shows the BSE pattern of the sample with x = 0 sintered at 1200 °C. In Fig. 2(a), some dark grains (Spot 1) and white grains (Spot 2) are observed. Further analysis of the composition of these grains was carried out through EDS analysis, with the corresponding results depicted in Fig. 2(b) and (c). As shown in Fig. 2(b) and (c), the EDS analysis reveals that the ratio of the sum of Ca and Sr content to Ti content in Spot 2 is 1:1, and there are no Zn and Mg elements. Combining XRD and EDS analysis, the white blocky morphology (Spot 2) corresponds to the secondary phase $Ca_{0.5}Sr_{0.5}TiO_3$. Conversely, Spot 1 contains almost no Ca and Sr elements but a higher amount of Zn and Mg elements (Li elements cannot be detected by EDS). Combining XRD and EDS analysis, the dark region (Spot 1) mainly corresponds to the main phase (Zn, Mg, Li)TiO_3 which contains Zn and Mg elements. Since diffraction peaks matching $MgTi_2O_5$ and Mg_2TiO_4 were observed in XRD patterns (x = 0.4). BSE and EDS analyses were used to further confirm the phase composition of $(Mg_{1/2}Zn_{1/2})_{0.4+x}Li_{0.4}(Ca_{1/2}Sr_{1/2})_{0.4-x}TiO_3$ ceramics at x = 0.4. As shown in Fig. 2(d)-(f), the ratio of the sum of Zn and Mg elements to Ti elements in Spot 4 is 11:13, respectively (Li elements were undetectable). Therefore, Spot 4 correspond to the main phase (Zn, Mg, Li)TiO_3. In Spot 3, the Ti content is significantly higher than that of Zn and Mg, indicating it is likely the $MgTi_2O_5$ phase. The relevant chemical reaction equations are as follows [16,26]:

$$2ZnO + 3TiO_2 \rightarrow Zn_2Ti_3O_8 \quad (10)$$

$$Zn_2Ti_3O_8 \rightarrow 2ZnTiO_3 + TiO_2 \quad (11)$$

$$3MgO + 3TiO_2 \rightarrow MgTiO_3 + MgTi_2O_5 + MgO \quad (12)$$

$$MgTiO_3 + MgO \rightarrow Mg_2TiO_4 \quad (13)$$

For further analysis of the structure of the $(Mg_{1/2}Zn_{1/2})_{0.4+x}Li_{0.4}(Ca_{1/2}Sr_{1/2})_{0.4-x}TiO_3$ ceramics, Fig. 3 shows the refined patterns for the samples (x = 0, x = 0.35) sintered at 1200 °C (Other refined patterns are listed in *Supplementary material* Fig. S1). Fig. 3 shows a good correlation between the observed XRD data and the fitting curve. The results indicate that the phase composition analysis obtained through XRD patterns is reasonable, and the crystal structure parameters are shown in Table 1 (Atomic occupation coordinates see Table S1 in *Supplementary Material*). In Table 1, the cell volume changes very slightly with increasing x value. Hence, it aligns with the finding that there was no notable shift observed in the diffraction peaks within the XRD patterns.

Table 1. Crystal structure parameters of $(Mg_{1/2}Zn_{1/2})_{0.4+x}Li_{0.4}(Ca_{1/2}Sr_{1/2})_{0.4-x}TiO_3$ ($0 \leq x \leq 0.375$) ceramics sintered at 1200 °C were obtained from the Rietveld refinement pattern results

	x	0	0.1	0.2	0.3	0.325	0.35	0.375
(Zn, Mg,Li)TiO_3	a=b=c (Å)	8.399	8.399	8.401	8.402	8.401	8.401	8.399
	V (Å^3)	592.3	592.4	592.7	593.1	592.99	592.9	592.4
	wt%	45.27	68.84	76.63	79.69	81.88	91.91	95.09
$Ca_{0.5}Sr_{0.5}TiO_3$	wt%	54.73	31.16	23.37	20.31	18.12	8.09	4.91
	χ^2	1.86	2.77	3.29	3.02	3.41	2.50	3.45

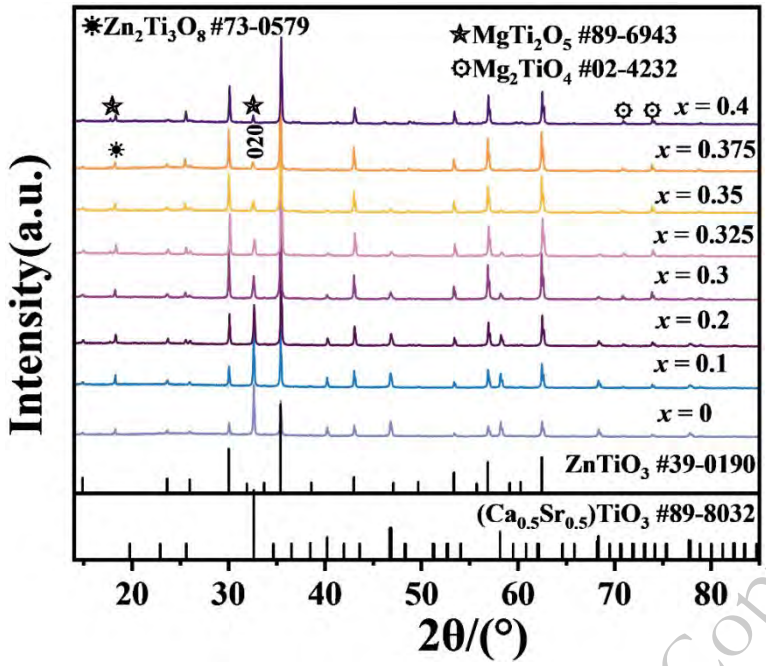

Fig. 1. XRD patterns of the high-entropy $(Mg_{1/2}Zn_{1/2})_{0.4+x}Li_{0.4}(Ca_{1/2}Sr_{1/2})_{0.4-x}TiO_3$ ($0 \le x \le 0.4$) ceramics sintered at 1200 ℃ for 4 h.

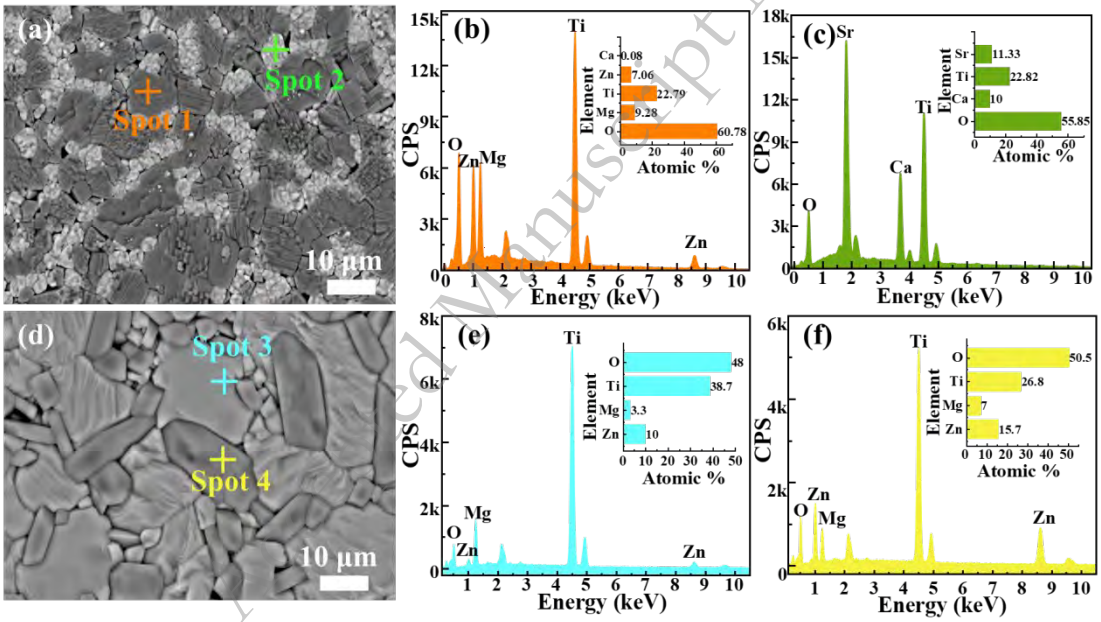

Fig. 2. (a) is BSE pattern of $(Mg_{1/2}Zn_{1/2})_{0.4+x}Li_{0.4}(Ca_{1/2}Sr_{1/2})_{0.4-x}TiO_3$ (x = 0) ceramics sintered at 1200 ℃ for 4 h; (b) and (c) are EDS results of Spot 1 and Spot 2; (d) is BSE pattern of $(Mg_{1/2}Zn_{1/2})_{0.4+x}Li_{0.4}(Ca_{1/2}Sr_{1/2})_{0.4-x}TiO_3$ (x = 0.4) ceramics sintered at 1200 ℃ for 4 h; (e) and (f) are EDS results of Spot 3 and Spot 4.

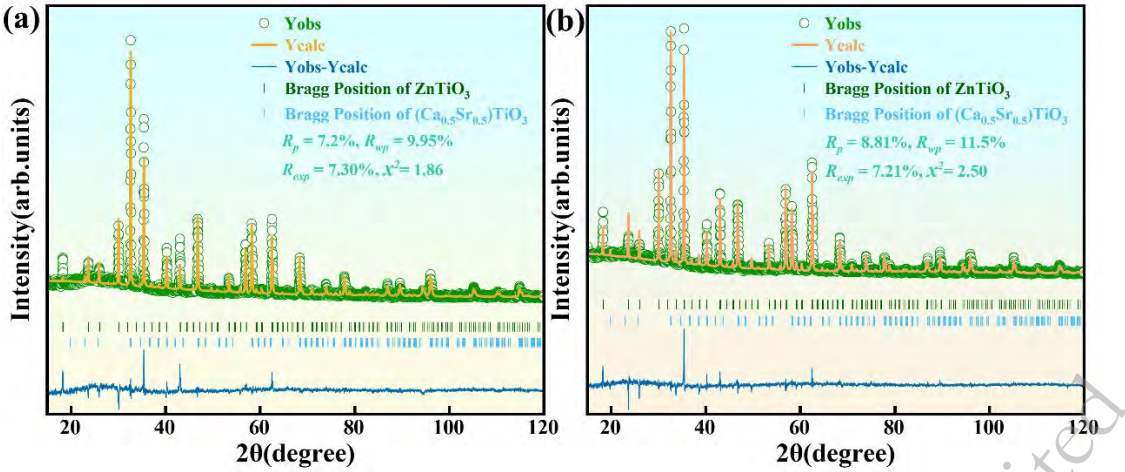

Fig. 3. Rietveld refinement of the XRD patterns for $(Mg_{1/2}Zn_{1/2})_{0.4+x}Li_{0.4}(Ca_{1/2}Sr_{1/2})_{0.4-x}TiO_3$ ceramics sintered at 1200 °C for 4 h: (a) x = 0 and (b) x = 0.35.

3.2. Microstructure

The SEM images in Fig. 4(a)-(c) depict the microstructure of $(Mg_{1/2}Zn_{1/2})_{0.4+x}Li_{0.4}(Ca_{1/2}Sr_{1/2})_{0.4-x}TiO_3$ (x = 0, 0.35, 0.4) ceramics sintered at 1200 °C for 4 h. All samples exhibited good densification without any liquid phase formation. The grains appeared in a layered structure, possibly originating from dislocations during the crystallization process [27]. The average particle size was calculated using Nano Measurer software. Compared to the x = 0 sample, the average particle size of the x = 0.35 sample exhibited a slight decrease. In Fig. 4(a)-(b), it is shown that as the x value increases from 0 to 0.35, the grains embedded within the layered structure become smaller, resulting in improved densification of the samples. Additionally, the crystallite size (D) of the samples can be obtained from the following Scherrer's equation [28]:

$$D = \frac{K\lambda}{\beta cos\theta} \tag{14}$$

where β is the full width at half maximum (FWHM), K is the shape factor (0.94), λ is the wavelength of X-rays (Cu K_α radiation, 1.5406 Å), and θ is the Bragg angle. As shown in Fig. 4(d), the trend in crystallite size corresponds with the unit cell size. This aligns with the expected relative density calculated.

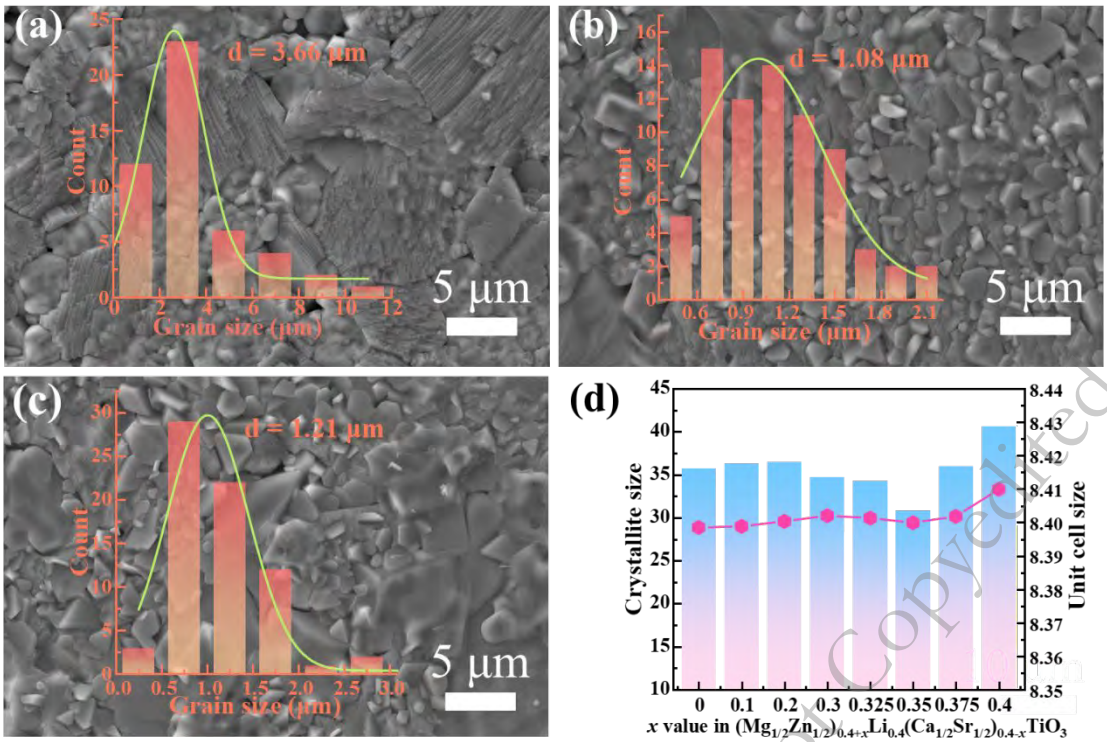

Fig. 4. SEM images of $(Mg_{1/2}Zn_{1/2})_{0.4+x}Li_{0.4}(Ca_{1/2}Sr_{1/2})_{0.4-x}TiO_3$ ceramics (a) x = 0, (b) x = 0.35, (c) x = 0.4 sintered at 1200 °C, respectively; (d) Crystallite size and the unit cell size.

3.3. Microwave dielectric properties

3.3.1. Dielectric constant analysis

Fig. 5(a) depicts the relationship between the dielectric constant (ε_r) and the x value for $(Mg_{1/2}Zn_{1/2})_{0.4+x}Li_{0.4}(Ca_{1/2}Sr_{1/2})_{0.4-x}TiO_3$ ($0 \le x \le 0.4$) ceramics. As the x value increases, there is a decreasing trend in the ε_r value of the samples. The ε_r value of the samples decreases from 60 to 17.6 within the range of $0 \le x \le 0.4$. The polarization capability of microwave dielectric ceramics is commonly represented by ε_r, typically primarily dependent on the secondary phase, ionic polarizability, and the densification degree (relative density) of the samples [19–31]. Fig. 5(b) illustrates the correlation between the ε_r value and molecular polarizability (α_T) at 1200 °C. The curves of ε_r values and α_T values are generally consistent and both exhibit a decreasing trend. According to the Shannon additive rule [26], because the ionic polarizabilities of Ca^{2+} and Sr^{2+} (3.16 Å^3, 4.24 Å^3) are greater than those of Zn^{2+} and Mg^{2+} (2.04 Å^3, 1.32 Å^3). With an increase in the x value, the concentration of Ca^{2+} and Sr^{2+} progressively

diminishes, leading to a monotonic decrease in molecular polarizability:

$$\alpha_{\mathrm{T}} = (0.4+x)\alpha[(\mathrm{Mg}_{1/2}\mathrm{Zn}_{1/2})^{2+}] + 0.4\alpha(\mathrm{Li}^{+}) + (0.4-x)\alpha[(\mathrm{Ca}_{1/2}\mathrm{Sr}_{1/2})^{2+}] + \alpha(\mathrm{Ti}^{4+}) + 3\alpha(\mathrm{O}^{2-}) \quad (15)$$

here, α_T represents the molecular polarizability. According to the Clausius-Mosotti equation in equation (11), the ε_r value is influenced by α_T [32]:

$$\varepsilon_{th} = \frac{3V_m + 8\pi\alpha_T}{3V_m - 4\pi\alpha_T} \quad (16)$$

where the theoretical dielectric constant, denoted as ε_{th}, and molar volume, represented by V_m, are the parameters involved. Additionally, due to the similar perovskite structure between $SrTiO_3$ and $CaTiO_3$, $Ca_{0.5}Sr_{0.5}TiO_3$ (ε_r = 240) also exhibits excellent dielectric properties [33,34]. To further analyze the effect of $Ca_{0.5}Sr_{0.5}TiO_3$ on the dielectric constant (ε_r) of $(Mg_{1/2}Zn_{1/2})_{0.4+x}Li_{0.4}(Ca_{1/2}Sr_{1/2})_{0.4-x}TiO_3$ ($0 \leq x \leq 0.4$) ceramics. The following Lichtenecker logarithmic rule is used to calculate the dielectric constant (ε_r) of $(Mg_{1/2}Zn_{1/2})_{0.4+x}Li_{0.4}(Ca_{1/2}Sr_{1/2})_{0.4-x}TiO_3$ ceramics [35]:

$$\ln \varepsilon_r = V_1 \ln \varepsilon_{r1} + V_2 \ln \varepsilon_{r2} \quad (17)$$

where V_1, V_2, ε_{r1}, and ε_{r2} respectively represent the volume fractions and dielectric constants of each phase in the multiphase system. In this study, the secondary phase $Ca_{0.5}Sr_{0.5}TiO_3$ (ε_r = 240) exhibits a much higher ε_r compared to the main phase $ZnTiO_3$ (ε_r = 17). According to equation (12), as x increases, the content of the high dielectric constant $Ca_{0.5}Sr_{0.5}TiO_3$ phase decreases, leading to a decrease in the overall dielectric constant of $(Mg_{1/2}Zn_{1/2})_{0.4+x}Li_{0.4}(Ca_{1/2}Sr_{1/2})_{0.4-x}TiO_3$ ceramics.

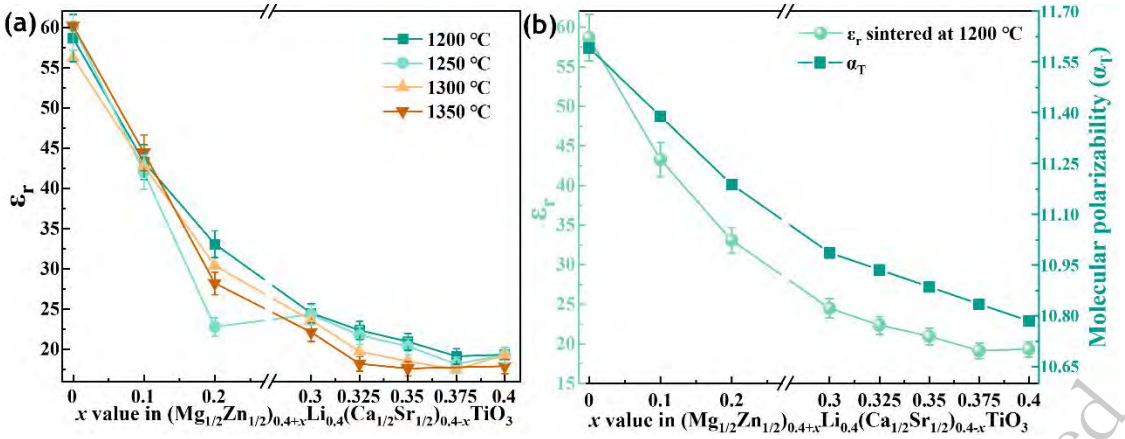

Fig. 5. (a) ε_r of $(Mg_{1/2}Zn_{1/2})_{0.4+x}Li_{0.4}(Ca_{1/2}Sr_{1/2})_{0.4-x}TiO_3$ ($0 \leq x \leq 0.4$) ceramics sintered at different temperatures for 4 h; (b) The influence of α_T on ε_r.

Fig. 6(a) illustrates the relationship between the dielectric constant ε_r and frequency for $(Mg_{1/2}Zn_{1/2})_{0.4+x}Li_{0.4}(Ca_{1/2}Sr_{1/2})_{0.4-x}TiO_3$ ($0 \leq x \leq 0.4$) ceramics at room temperature. The dielectric constant remains nearly unchanged with frequency, indicating good stability over a wide frequency range. Previous studies suggest that this stability could be attributed to entropy stabilization, as literature has reported the influence of configurational entropy on electrochemical and thermal stability [36]. The variation of dielectric loss with frequency is depicted in Fig. 6(b). The dielectric loss of $(Mg_{1/2}Zn_{1/2})_{0.4+x}Li_{0.4}(Ca_{1/2}Sr_{1/2})_{0.4-x}TiO_3$ ($0 \leq x \leq 0.4$) ceramics notably decreases near 20 kHz. Additionally, the dielectric loss of the samples decreases with increasing x value, possibly correlated with phase transitions and structural stability of the ceramics [36].

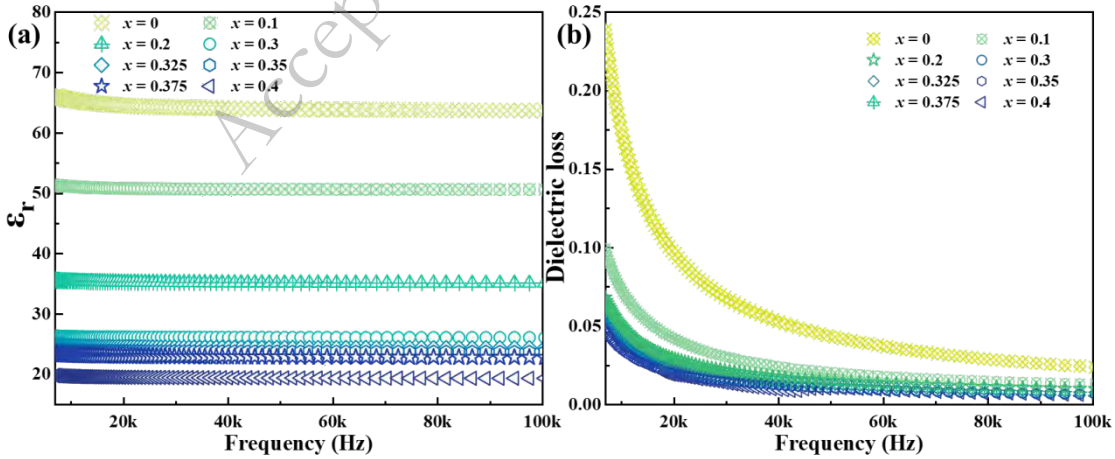

Fig. 6. Dielectric dispersion spectra of $(Mg_{1/2}Zn_{1/2})_{0.4+x}Li_{0.4}(Ca_{1/2}Sr_{1/2})_{0.4-x}TiO_3$ ($0 \leq x \leq 0.4$) ceramics sintered at 1200 °C for 4 h measured at room temperature: (a) dielectric constant, (b) dielectric loss.

3.3.2. Quality factor analysis

The relationship between the *Qf* value of $(Mg_{1/2}Zn_{1/2})_{0.4+x}Li_{0.4}(Ca_{1/2}Sr_{1/2})_{0.4-x}TiO_3$ ceramics and *x* value at sintering temperatures of 1200 °C - 1350 °C is shown in Fig. 7(a). Densification, secondary phase, and grain boundaries affect the *Qf* value externally, while internally, factors like defects, cation disorder, and lattice vibrations, among others, also have an impact [37,38]. The *Qf* value of the samples rises steadily with increasing *x* value, and the change in *Qf* value closely follows the trend of relative density until $x = 0.325$. The increase in relative density of the samples ($0 \leq x \leq 0.325$) indicates a decrease in porosity, and consequently, the *Qf* values of the samples also increase. Between the *x* values of 0.325 and 0.35, a slight decline in the relative density of the samples is observed. However, during this period, the *Qf* value of the $(Mg_{1/2}Zn_{1/2})_{0.4+x}Li_{0.4}(Ca_{1/2}Sr_{1/2})_{0.4-x}TiO_3$ ceramics continues to increase. This is attributed to an increase in the content of the (Zn, Mg, Li)TiO_3 phase with a high *Qf* value (*Qf* = 40,000 GHz), and a decrease in the content of the $Ca_{0.5}Sr_{0.5}TiO_3$ phase with low *Qf* value (*Qf* = 4,100 GHz) [33,39], as shown in Fig. 7(b). In multiphase ceramic systems, the *Qf* value can be estimated using the provided mixing rules [16]:

$$(Qf)^{-1} = V_1 (Qf)_1^{-1} + V_2 (Qf)_2^{-1} \quad (18)$$

where V_1, V_2, $(Qf)_1$, and $(Qf)_2$ respectively represent the volume fractions and the *Qf* value of each phase. Based on the equations above, increasing the proportion of the (Zn, Mg, Li)TiO_3 phase, which has higher *Qf* values, improves the overall *Qf* value of the $(Mg_{1/2}Zn_{1/2})_{0.4+x}Li_{0.4}(Ca_{1/2}Sr_{1/2})_{0.4-x}TiO_3$ ceramics. Additionally, this indicates that the positive effect of the secondary phase outweighs the impact of the decrease in density.

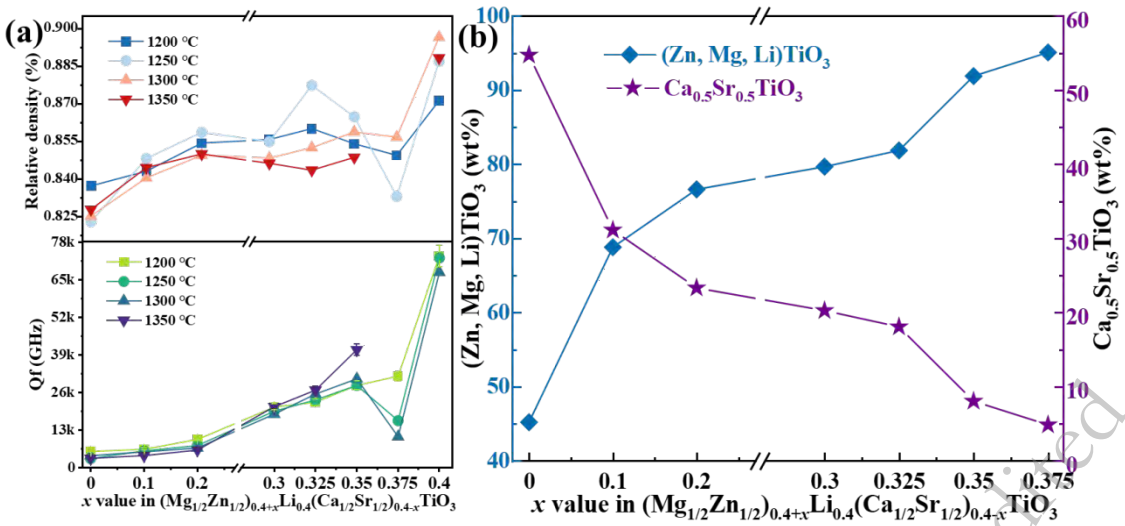

Fig. 7. (a) The *Qf* value of $(Mg_{1/2}Zn_{1/2})_{0.4+x}Li_{0.4}(Ca_{1/2}Sr_{1/2})_{0.4-x}TiO_3$ ($0 \le x \le 0.4$) ceramics sintered at different temperature for 4 h; (b) The weight fraction of the main phase (Zn, Mg, Li)TiO_3 and the secondary phase $Ca_{0.5}Sr_{0.5}TiO_3$.

3.3.3. Temperature coefficient of resonant frequency analysis

The variation trend of the τ_f value for $(Mg_{1/2}Zn_{1/2})_{0.4+x}Li_{0.4}(Ca_{1/2}Sr_{1/2})_{0.4-x}TiO_3$ ceramics ($0 \le x \le 0.4$) is depicted in Fig. 8(a). The τ_f value of samples at different sintering temperatures exhibits a monotonic decreasing trend as x increases, transitioning from positive to negative values. Given that the τ_f curve crosses zero, this suggests that adjusting the x value appropriately can yield samples with τ_f nearing zero. Generally, the τ_f value of most microwave dielectric ceramics is influenced by their crystal structure and secondary phases [40–41]. The distortion of the $[AO_6]$ octahedron is caused by five atoms, Mg, Zn, Li, Ca, and Sr, randomly occupying the A-site of the $(Mg_{1/2}Zn_{1/2})_{0.4+x}Li_{0.4}(Ca_{1/2}Sr_{1/2})_{0.4-x}TiO_3$ ceramics. As x increases, individual bond lengths of $[AO_6]$ octahedron in $(Mg_{1/2}Zn_{1/2})_{0.4+x}Li_{0.4}(Ca_{1/2}Sr_{1/2})_{0.4-x}TiO_3$ ceramics change, resulting in octahedron distortion (Δ_{octa}). The extent of Δ_{octa} can be evaluated by the following equation [8]:

$$\Delta_{octa} = \frac{1}{6}\sum_{i}\left(\frac{R_{i-o} - R_{ave}}{R_{ave}}\right)^2 \quad (19)$$

the average bond length between cations and oxygen ions in the oxygen octahedron is represented by R_{ave}, whereas R_i represents individual bond lengths. The relationship

between the τ_f value and Δocta is illustrated in Fig. 8(b). When $0 \leq x \leq 0.2$, as Δocta decreases, the τ_f value moves in a positive direction. The reduction in τ_f values is influenced by the decrease in [AO_6] octahedron distortion, as the reduced thermal energy should be absorbed to restore the [AO_6] octahedron distortion rather than to restore the temperature dependence of polarization. With further increase in x values, when $0.2 \leq x \leq 0.375$, Δ_{octa} slightly increases, but τ_f values continue to move towards the positive direction. This is because the τ_f value of $Ca_{0.5}Sr_{0.5}TiO_3$ (1,200 ppm/°C) [33] is much larger than that of (Zn, Mg, Li)TiO_3 (about -55 ppm/°C) [42]. When $0.2 \leq x \leq 0.375$, as the mass fraction of the second phase $Ca_{0.5}Sr_{0.5}TiO_3$ decreases, it enables the τ_f value of $(Mg_{1/2}Zn_{1/2})_{0.4+x}Li_{0.4}(Ca_{1/2}Sr_{1/2})_{0.4-x}TiO_3$ ceramics to approach zero within a certain range. The τ_f value for multiphase ceramics can be obtained via the mixing rule [18,43]:

$$\tau_f = V_1\tau_{f1} + V_2\tau_{f2} \tag{20}$$

here, in the multiphase ceramics system, V_1 and V_2 represent the volume fractions of each phase, while τ_{f1} and τ_{f2} denote the temperature coefficients of resonant frequency for each phase.

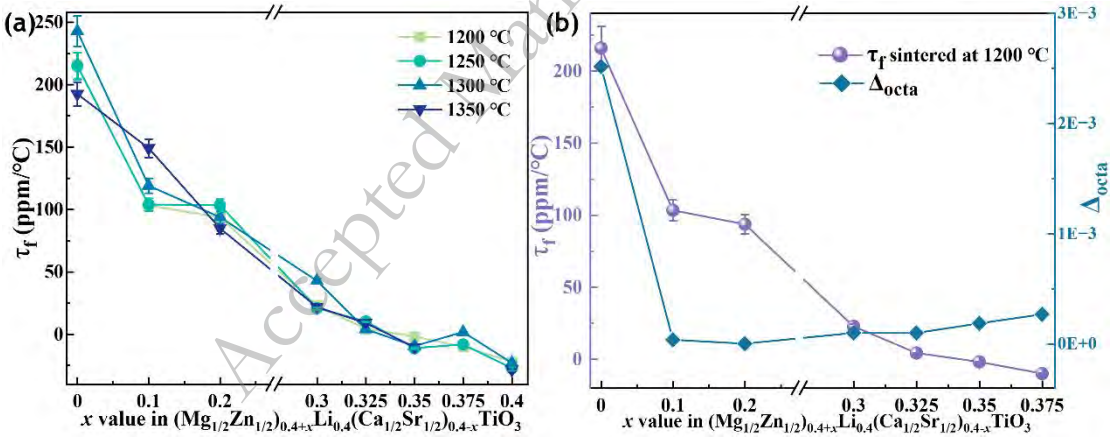

Fig. 8. (a) τ_f of $(Mg_{1/2}Zn_{1/2})_{0.4+x}Li_{0.4}(Ca_{1/2}Sr_{1/2})_{0.4-x}TiO_3$ ($0 \leq x \leq 0.4$) ceramics sintered at different temperatures for 4 h; (b) The influence of Δ_{octa} on τ_f.

Considering the microwave dielectric properties, particularly ε_r and *Qf*, which are significantly affected by the sintering temperature, relevant analyses have been conducted (see Fig. S2 in *Supplementary material*). In the process of practicalizing

microwave dielectric ceramics, the τ_f value is an essential factor to consider, playing a crucial role in material selection and design. Fig. 9 demonstrates the variation of the τ_f value with sintering temperature for $(Mg_{1/2}Zn_{1/2})_{0.4+x}Li_{0.4}(Ca_{1/2}Sr_{1/2})_{0.4-x}TiO_3$ ceramics and other MT-based microwave dielectric ceramics [12,44–51]. From Fig. 9, it can be observed that the τ_f value of $MgTiO_3$ can be significantly improved through high-entropy design. Particularly, when x = 0.35, the τ_f value of $(Mg_{1/2}Zn_{1/2})_{0.4+x}Li_{0.4}(Ca_{1/2}Sr_{1/2})_{0.4-x}TiO_3$ ceramic is -8.6 ppm/°C. This highlights the potential of high-entropy design in enhancing microwave dielectric performance and offers promising prospects for practical applications.

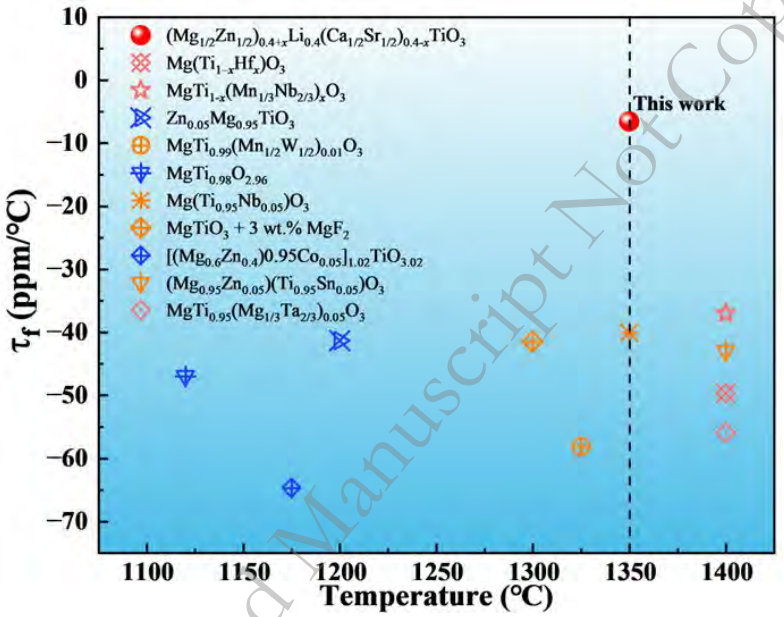

Fig. 9. The τ_f and sintering temperatures from this work and other reported MT-based ceramics are summarized.

4. Conclusions

$(Mg_{1/2}Zn_{1/2})_{0.4+x}Li_{0.4}(Ca_{1/2}Sr_{1/2})_{0.4-x}TiO_3$ ($0 \leq x \leq 0.4$) ceramics were synthesized in this study through the conventional solid-state reaction method at a sintering temperature ranging from 1200 °C to 1350 °C. Discussed in this study was the impact of high-entropy design on the sintering behavior, phase composition, microstructure, and microwave dielectric properties of $(Mg_{1/2}Zn_{1/2})_{0.4+x}Li_{0.4}(Ca_{1/2}Sr_{1/2})_{0.4-x}TiO_3$ ceramics, with a focus on the non-equimolar ratio of Mg-site. Based on the XRD

patterns, Rietveld refinement results, and EDS analysis, it was observed that (Zn, Mg, Li)TiO_3 was the main phase, and $Ca_{0.5}Sr_{0.5}TiO_3$ was the secondary phase for $0 \leq x \leq 0.375$. The *Qf* value of the samples depends mainly on the densification and the presence of the $Ca_{0.5}Sr_{0.5}TiO_3$ phase. The impact factors of the ε_r value are attributed to molecular polarizability and the secondary phase $Ca_{0.5}Sr_{0.5}TiO_3$. The τ_f value exhibited a close correlation with [AO_6] octahedron distortion and the secondary phase with a positive τ_f value. Specifically, $(Mg_{1/2}Zn_{1/2})_{0.4+x}Li_{0.4}(Ca_{1/2}Sr_{1/2})_{0.4-x}TiO_3$ (x = 0.35) ceramics demonstrated optimal microwave dielectric properties: ε_r = 17.6, *Qf* = 40,900 GHz, τ_f = -8.6 ppm/°C. Therefore, $(Mg_{1/2}Zn_{1/2})_{0.4+x}Li_{0.4}(Ca_{1/2}Sr_{1/2})_{0.4-x}TiO_3$ ceramics demonstrate significant potential for future millimeter-wave communication applications.

Acknowledgements

This research was funded by the Sichuan Science and Technology Program (No. 2023YFQ0082). Guangdong Provincial Key Laboratory of Electronic Functional Materials and Device (No. EFMD2022005Z). State Key Laboratory of Advanced Technologies for Comprehensive Utilization of Platinum Metals (No. SKL-SPM-202021).

References

[1] B. Liu, L. Li, K.X. Song, M.M. Mao, Z. Lu, G. Wang, L. Li, D. Wang, D. Zhou, A. Feteira, and I.M. Reaney, Enhancement of densification and microwave dielectric properties in LiF ceramics via a cold sintering and post-annealing process, *J. Eur Ceram Soc*., 41(2021), No. 2, p. 1726.

[2] K. Liu, C.Liu, J. Li, L. Jin, and H. Zhang, Relationship between structure and properties of microwave dielectric ceramic $Li_{(1+x)2}MgTi_3O_8$ based on Li non-stoichiometry, *J Materiomics*., (9)2023, No. 2, p. 279.

[3] Q. Zhang, X. Tang, F. Huang, X. Wu, Y. Li, and H. Su, Enhanced microwave dielectric properties of wolframite structured $Zn_{1-x}Cu_xWO_4$ ceramics with low sintering temperature, *J Materiomics*., (7)2021, No. 6, p. 1309.

[4] B.R. Ke, Y.C Sun, Y. Zhang, W.R. Wang, W.M. Wang, P.Y. Ma, W. Ji, and Z.Y. Fu, Powder metallurgy of high-entropy alloys and related composites: A short review, *Int J Min Met Mater*., 28(2021), No. 6, p. 931.

[5] Y. Lu, Y. Dong, S. Guo, L. Jiang, H. Kang, T. Wang, B. Wen, Z. Wang, J. Jie, Z. Cao, H. Ruan, and T. Li, A promising new class of high-temperature alloys: Eutectic high-entropy alloys, *Sci Rep*., 4(2014), art. No. 6200.

[6] Z. Lei, X. Liu, H. Wang, Y. Wu, S. Jiang, and Z. Lu, Development of advanced materials via entropy engineering, *Scr Mater*., 165(2019), p. 164.

[7] Q. Guo, X. Xu, X. Pei, Z. Duan, P.K. Liaw, H. Hou, and Y. Zhao, Predict the phase formation of high-entropy alloys by compositions, *J Mater Res Technol*., 22(2023), p. 3331.

[8] K. Liu, H. Zhang, C. Liu, J. Li, L. Shi, X. Wang, and D. Zhang, Crystal structure and microwave dielectric properties of $(Mg_{0.2}Ni_{0.2}Zn_{0.2}Co_{0.2}Mn_{0.2})_2SiO_4$-A novel high-entropy ceramic, *Ceram Int*., 48(2022), No.16, p. 23307.

[9] X. Zhang, X. Liu, J. Yan, Y. Gu, and X. Qi, Preparation and Property of High-entropy $(La_{0.2}Li_{0.2}Ba_{0.2}Sr_{0.2}Ca_{0.2})TiO_3$ Perovskite Ceramics, *J Inorg Mater*., 36(2021), No. 4, p. 379.

[10] H. Xiang, L. Yao, J. Chen, A. Yang, H. Yang, and L. Fang, Microwave dielectric high-entropy ceramic $Li(Gd_{0.2}Ho_{0.2}Er_{0.2}Yb_{0.2}Lu_{0.2})GeO_4$ with stable temperature coefficient for low-temperature cofired ceramic technologies, *J Mater Sci Technol*., 93(2021), p. 28.

[11] E.S. Kim and C.J. Jeon, Microwave dielectric properties of $ATiO_3$ (A = Ni, Mg, Co, Mn) ceramics, *J Eur Ceram Soc*., 30(2010), No. 2, p. 341.

[12] J. Zhang, Z. Yue, Y. Luo, and L. Li, $MgTiO_3/TiO_2/MgTiO_3$: An ultrahigh-Q and temperature-stable microwave dielectric ceramic through cofired trilayer architecture, *Ceram Int*., 44(2018), No. 17, p. 21000.

[13] J.S. Chung and E.S. Kim, Improvement of Microwave Dielectric Properties of $MgTiO_3$ Ceramics by Ti-Site Complex Substitution, *Electron Mater Lett.*, 20(2024), No. 1, p. 56.

[14] S. Filipović, V.P. Pavlović, N. Obradović, V. Paunović, K. Maca, and V.B. Pavlović, The impedance analysis of sintered $MgTiO_3$ ceramics, *J Alloys Compd.*, 701(2017), p. 107.

[15] C. L. Huang and S. S. Liu, Dielectric characteristics of the $(1-x)Mg_2TiO_4$–$xSrTiO_3$ ceramic system at microwave frequencies, *J Alloys Compd.*, 471(2009), No. 1, p. L9.

[16] T. Shi, F. Zhang, W. Sun, J. Li, Y. Bai, C. Wang, X. Wang, Y. Yang, and Z.J. Wang, Fabrication, sinterability and microwave dielectric properties of $MgTiO3-(Ca_{0.8}Sr_{0.2})TiO_3$ composite ceramics from nanosized powders, *Vacuum.*, 201(2022), art. No. 111107.

[17] D. Bérardan, S. Franger, A.K. Meena, and N. Dragoe, Room temperature lithium superionic conductivity in high entropy oxides, *J Mater Chem A Mater.*, 4(2016), No. 24, p. 9536.

[18] C.L. Huang and S.S. Liu, Characterization of extremely low loss dielectrics $(Mg_{0.95}Zn_{0.05})TiO_3$ at microwave frequency, *Jpn J Appl Phys.*, 46(2007), No. 1, p. 283.

[19] C. Qi, F. Wang, Y. Lai, W. Gong, F. Huang, B. Li, X. Yang, R. Peng, C. Wu, and H. Su, Temperature Stability of Li_2TiO_3-Zn_2SiO_4 Microwave Dielectric Ceramics, *Eur J Inorg Chem.*, 2022(2022), No. 29, art. No. e202200380.

[20] X. Li, X. Yang, Y. Lai, Q. Zhang, B. Li, C. Qi, J. Yin, F. Wang, C. Wu, and H. Su, Improved microwave dielectric properties of $MgAl_2O_4$ spinel ceramics through $(Li_{1/3}Ti_{2/3})^{3+}$ doping, *Chinese Phys B.*, 32(2023), No. 5, art. No. 057701.

[21] B. Ullah, W. Lei, Y.F. Yao, X.C. Wang, X.H. Wang, M. Ur-Rahman, and W.Z. Lu, Structure and synergy performance of $(1-x)Sr_{0.25}Ce_{0.5}TiO_{3-x}La(Mg_{0.5}Ti_{0.5})O_3$ based microwave dielectric ceramics for 5G architecture, *J Alloys Compd.*, 763(2018), p. 990.

[22] X. Yang, Y. Lai, Y. Zeng, F. Yang, F. Huang, B. Li, F. Wang, C. Wu, and H. Su, Spinel-type solid solution ceramic $MgAl_2O_4$-Mg_2TiO_4 with excellent microwave dielectric properties, *J Alloys Compd.*, 898(2022), art. No. 162905.

[23] F. Wang, Y. Lai, Q. Zhang, X. Yang, B. Li, C. Wu, H. Su, and G. Jiang, Improved microwave dielectric properties of $(Mg_{0.5}Ti_{0.5})^{3+}$ Co-substituted $Mg_2Al_4Si_5O_{18}$ cordierite ceramics, *Solid State Sci*., 132(2022), art. No. 106989.

[24] J. Yang and J.H. Swisher, The Phase Stability of $Zn_2Ti_30_8$, *Mater Charact*., 37(1996), No. 2, p. 153.

[25] W. Liao, J. Tian, Z. Shan, R. Na, L. Cui, and H. Lin, Facile synthesis of $Zn_2Ti_3O_8$ hollow spheres based on ion exchange as promising anodes for lithium ion batteries, *Electrochim Acta*., 216(2016) , p. 94.

[26] B. Li, Y. Lai, Y. Zeng, F. Yang, F. Huang, X. Yang, F. Wang, C. Wu, X. Zhong, and H. Su, Structure and microwave dielectric properties of $(Zn_{1/3}Nb_{2/3})^{4+}$ Co-substituted $MgTiO_3$ ceramic, *Mat Sci Eng B.*, 276(2022), art. No. 115572.

[27] A. Zhang, H. Fan, D. Hou, F. Yang, Y. Chen, W. Wang, and W. Dong, A novel low-loss $(1\text{-}x)(Ca_{0.8}Sr_{0.2})TiO_{3\text{-}x}SmAlO_3$ microwave dielectric ceramics with near-zero temperature coefficient, *J Alloys Compd*., 898(2022), art. No. 162809.

[28] M.R. Parra and F.Z. Haque, Aqueous chemical route synthesis and the effect of calcination temperature on the structural and optical properties of ZnO nanoparticles, *J Mater Res Technol*., 3(2014), No. 4, p. 363.

[29] Z. Liu, S. Xu, T. Li, B. Xie, K. Guo, and J. Lu, Microstructure and ferroelectric properties of high-entropy perovskite oxides with A-site disorder, *Ceram Int*., 47 (2021), No. 23, p. 33039.

[30] T. Su, H. Chen, Z. Wei, M. Hao, X. Wang, Y. Liu, C. Ma, Y. Miao, and F. Gao, Structure and microwave dielectric properties of Al^{3+}-doped $(Zn_{1/6}Ba_{1/6}Ca_{1/6}Sr_{1/6}La_{1/3})TiO_3$ high-entropy ceramics system, *Ceram Int*., 50(2024), No. 3, p. 5043.

[31] J. Li, X.K. Lan, K. Du, X.Q. Song, W.Z. Lu, G.F. Fan, and W. Lei, Crystal structure and temperature dependence of permittivity in barium aluminate based solid solutions, *J Am Ceram Soc*., 102(2019), No. 12, p. 7480.

[32] R.D. Shannon, Dielectric polarizabilities of ions in oxides and fluorides, *J Appl Phys*., 73(1993), No. 1, p. 348.

[33] C. Chen, Z. Peng, L. Xie, K. Bi, and X. Fu, Microwave dielectric properties of novel $(1-x)MgTiO_3–xCa_{0.5}Sr_{0.5}TiO_3$ ceramics, *J Mater Sci-Mater El*., 31(2020), No. 16, p. 13696.

[34] T. Luo, X. Shan, J. Zhao, H. Feng, Q. Zhang, H. Yu, and J. Liu, Improvement of quality factor of $SrTiO_3$ dielectric ceramics with high dielectric constant using Sm_2O_3, *J Am Ceram Soc*., 102(2019), No. 7, p. 3849.

[35] K.P. Surendran, N. Santha, P. Mohanan, and M.T. Sebastian, Temperature stable low loss ceramic dielectrics in $(1-x)ZnAl_2O_{4-x}TiO_2$ system for microwave substrate applications, *Eur Phys J*., 41(2004), No. 3, p. 301.

[36] S. Zhou, Y. Pu, Q. Zhang, R. Shi, X. Guo, W. Wang, J. Ji, T. Wei, and T. Ouyang, Microstructure and dielectric properties of high entropy $Ba(Zr_{0.2}Ti_{0.2}Sn_{0.2}Hf_{0.2}Me_{0.2})O_3$ perovskite oxides, *Ceram Int*., 46(2020), No. 6, p. 7430.

[37] X. Zhu, F. Kong, and X. Ma, Sintering behavior and properties of $MgTiO_3$/CaO-B_2O_3-SiO_2 ceramic composites for LTCC applications, *Ceram Int*., 45(2019), No. 2, p. 1940.

[38] X.H. Wang, M.L. Mu, H. Jiang, W. Lei, and W.Z. Lu, Investigation on structure and microwave dielectric properties of novel high dielectric constant $Ca_{(1-3x/2)}Ce_xTiO_3$ ceramics sintered in nitrogen atmosphere, *J Mater Sci-Mater El*., 30(2019), No. 2, p. 1591.

[39] H.T. Kim, Y. Kim, M. Valant, and D. Suvorov, Titanium Incorporation in Zn_2TiO_4 Spinel Ceramics, *J Am Ceram Soc*., 84(2001), No. 5, p. 1081.

[40] T.H. Hsu and C.L. Huang, Microwave dielectric properties of ultra-low-temperature-sintered TiO_2 as a τ_f compensator, *Appl Phys A Mater Sci Process*., 129(2023), No. 1, art. No. 20.

[41] L. Cheng, P. Liu, S.X. Qu, L. Cheng, and H. Zhang, Microwave dielectric properties of Mg_2TiO_4 ceramics synthesized via high energy ball milling method, *J Alloys Compd*., 623(2015), p. 238.

[42] M. Wang, J. Zhou, Z. Yue, L. Li, and Z. Gui, Co-firing behavior of $ZnTiO_3$-TiO_2 dielectrics/hexagonal ferrite composites for multi-layer LC filters, *Mat Sci Eng B*., 2003, No. 1, p. 262.

[43] Y. Wu, D. Zhou, J. Guo, L.X. Pang, H. Wang, and X. Yao, Temperature stable microwave dielectric ceramic $0.3Li_2TiO_3$-$0.7Li(Zn_{0.5}Ti_{1.5})O_4$ with ultra-low dielectric loss, *Mater Lett*., 65(2011), No. 17, p. 2680.

[44] Z. Ren, F. Zeng, C. Yuan, F. Liu, J. Zhao, B. Zhu, C. Zhou, J. Xu, and G. Rao, Enhanced quality factor (~336,800 GHz) of $MgTiO_3$ ceramic by Hf substitution for Ti-site, *Ceram Int*., 50(2024), No. 6, p. 9861.

[45] K. Sharma and S. Bahel, Structural, dielectric and reflection analysis of $Zn_xMg_{1-x}TiO_3$ ceramics synthesized using auto-ignition combustion method, Journal of Materials Science: *J Mater Sci-Mater El*., 32(2021), No. 23, p. 27216.

[46] Z. Fang, H. Yang, H. Yang, Z. Xiong, X. Zhang, P. Zhao, and B. Tang, Ilmenite-type $MgTiO_3$ ceramics by complex $(Mn_{1/2}W_{1/2})^{4+}$ cation co-substitution producing improved microwave characteristics, *Ceram Int*., 47 (2021), No. 15, p. 21388.

[47] M. Wang and D. Yan, Improved crystalline structure and sintering characteristics of nonstoichiometric $MgTiO_3$ ceramics by sol–gel method, *J Solgel Sci Technol*., 97(2021), No. 2, p. 365.

[48] X. Jia, Y. Xu, P. Zhao, J. Li, and W. Li, Structural dependence of microwave dielectric properties in ilmenite-type $Mg(Ti_{1-x}Nb_x)O_3$ solid solutions by Rietveld refinement and Raman spectra, *Ceram Int*., 47(2021), No. 4, p. 4820.

[49] S. Yuan, L. Gan, F. Ning, S. An, J. Jiang, and T. Zhang, High-Q×f 0.95 $MgTiO_3$–0.05$CaTiO_3$ microwave dielectric ceramics with the addition of LiF sintered at medium temperatures, *Ceram Int*., 44(2018), No. 16, p. 20566.

[50] S.H. Lin and Y.B. Chen, Low dielectric loss characteristics of $[(Mg_{1-x}Zn_x)_{0.95}Co_{0.05}]_{1.02}TiO_{3.02}$ ceramics at microwave frequencies, *J Mater Sci-Mater El*., 28(2017), No. 5, p. 4154.

[51] H.J. Jo, J.S. Kim, and E.S. Kim, Microwave dielectric properties of $MgTiO_3$-based ceramics, *Ceram Int*., (41)2015, p. s530.